

# Bicontinuous porous membranes with micro-nano composite structure using a facile atomization-assisted nonsolvent induced phase separation method

Jing Wang<sup>1,2</sup>, Guoyuan Pan<sup>2</sup>, Yu Li<sup>1,2</sup>, Yang Zhang<sup>2</sup>, Hongwei Shi<sup>2</sup>, Xuanbo Liu<sup>2</sup>, Hao Yu<sup>2</sup>, Muhua Zhao<sup>2</sup>, Yiqun Liu (✉)<sup>1,2</sup>, Changjiang Wu (✉)<sup>1,2</sup>

1 College of Materials Science and Engineering, Beijing University of Chemical Technology, Beijing 100029, China

2 SINOPEC Beijing Research Institute of Chemical Industry, Beijing 100013, China

© Higher Education Press 2022

**Abstract** The micro-nano composite structure can endow separation membranes with special surface properties, but it often has the problems of inefficient preparation process and poor structural stability. In this work, a novel atomization-assisted nonsolvent induced phase separation method, which is also highly efficient and very simple, has been developed. By using this method, a bicontinuous porous microfiltration membrane with robust micro-nano composite structure was obtained via commercially available polymers of polyacrylonitrile and polyvinylpyrrolidone. The formation mechanism of the micro-nano composite structure was proposed. The microphase separation of polyacrylonitrile and polyvinylpyrrolidone components during the atomization pretreatment process and the hydrogen bonding between polyacrylonitrile and polyvinylpyrrolidone molecules should have resulted in the nano-protrusions on the membrane skeleton. The membrane exhibits superhydrophilicity in air and superoleophobicity underwater. The membrane can separate both surfactant-free and surfactant-stabilized oil-in-water emulsions with high separation efficiency and permeation flux. With excellent antifouling property and robust microstructure, the membrane can easily be recycled for long-term separation. Furthermore, the scale-up verification from laboratory preparation to continuous production has been achieved. The simple, efficient, cost-effective preparation method and excellent membrane properties indicate the great potential of the developed membranes in practical applications.

**Keywords** atomization, nonsolvent induced phase

separation, bicontinuous porous structure, micro-nano composite structure, oil-water separation

## 1 Introduction

Oil-water mixture and emulsified oil with catastrophic harm to ecological environment and human health are widely generated in many industrial processes, such as those seen in chemical, petroleum, food processing and machinery industries [1–3]. The common techniques used to treat oily wastewater with different droplet distributions include gravity sedimentation, centrifugal separation, adsorption, biological treatment, air flotation and membrane separation [4–11]. Among them, the membrane separation technology has attracted wide attention because of its advantages of low energy consumption, no secondary pollution, high separation accuracy, and simple operation [12–15].

The micro-nano composite structure in organisms, as found in nature, can give them special surface properties, such as the superwettability of some plant leaves (lotus leaf, duckweed leaf, etc.) and animal organs (cicada wings, shark skin, etc.) [16–18]. Generally speaking, two criteria are necessary for the design of a superwettable surface: appropriate surface free energy of the material itself and a micro/nanostructured rough microstructure [19–23]. To imitate these special structures, researchers have developed many preparation methods, such as self-assembly, laser ablation, grafting modification and electrospinning [24–27]. A lot of exploratory work in the field of superwettability separation membranes has been carried out based on material design and microstructure design, and resultantly the “oil-removing” type materials with superhydrophobicity/superoleophilicity and the “water-removing” type materials with superhydrophilicity/underwater

Received September 24, 2021; accepted November 12, 2021

E-mails: liuyq.bjhy@sinopec.com (Liu Y), wuchangjiang.bjhy@sinopec.com (Wu C)

superoleophobicity have been prepared [28–31]. However, the reported methods still face some problems, such as low production efficiency, complicated membrane material preparation process and unfavorable for large-scale production.

Regardless of whether the separation is for oil-rich emulsions or water-rich emulsions, high porosity ( $> 70\%$ ) and large pore diameter ( $> 0.1 \mu\text{m}$ ) are the key factors affecting the permeate flux and retention rate of the separation membrane in practical applications [32]. The typical method to obtain polymer membranes with such characteristics is electrospinning [33–36]. The obtained nanofiber membranes have the advantages of high specific surface area, high porosity, good permeability and desirable wettability. However, the complex operating conditions, difficulty in solvent recovery, high voltage risk, low production efficiency and inability to run for a long time seriously hinder its practical application [36,37]. Separation membranes with high porosity and large pore size can also be prepared by vapor induced phase separation (VIPS) [38,39]. In VIPS method, the nonsolvent penetrates from a vapor phase to polymer solution and induces phase separation, which is more similar to the nonsolvent induced phase separation (NIPS) method, but with a much slower mass transfer rate [40]. This can be attributed to the slower kinetics of gaseous nonsolvents in comparison to liquid nonsolvents used in NIPS [41–43]. The slower mass transfer speed can better control the morphology of the membrane. Although the preparation method of VIPS is simple and easy to control, the exposure time usually takes tens of minutes or even hours. The preparation process with such low production efficiency is undoubtedly unfavorable for continuous industrial production. Therefore, there is an urgent need for a simple, fast, and easy-to-scale production method for preparing an oil-water separation membrane with a micro-nano composite structure.

Herein, inspired by the delicate three-dimensional (3D) fiber network structure of loofah sponge, the microfiltration membranes with bicontinuous porous structures based on commercially available polymers polyacrylonitrile (PAN) and polyvinylpyrrolidone (PVP) were fabricated by a novel atomization-assisted NIPS method (AA-NIPS). Compared with electrospinning technology and VIPS, AA-NIPS has milder preparation conditions, simpler operation steps, better safety, and higher production efficiency. Surprisingly, the PAN/PVP membrane fabricated by using the AA-NIPS method also has nanoscale protrusions on the entire fibrous skeleton when the suitable process parameters are chosen, which provides a new way for obtaining micro/nanoscale hierarchical structure. Different from the traditional VIPS method, the high humidity vapor environment of VIPS is replaced by a micron-scale atomized water-droplet bath in the AA-NIPS method. The nonsolvent precipitant infiltration rate into the nascent cast film is accelerated due to the replacement of

water vapor molecules with atomized water droplets, but this precipitant infiltration rate is still much lower than that in NIPS method. The slow introduction of nonsolvent leads to uniform and flat precipitant concentration profiles in the cast film, and a more-or-less homogenous structure is obtained in the final membrane. The prepared PAN/PVP membrane has ultra-low oil adhesion and underwater superoleophobicity due to its micro/nanoscale hierarchical structure. The membrane can separate both surfactant-free and surfactant-stabilized oil-in-water emulsions under a small applied pressure (10 kPa), with high separation efficiency (99.8%) and high flux (up to  $3700 \text{ L} \cdot \text{m}^{-2} \cdot \text{h}^{-1}$ ). The outstanding performance of the membrane for the separation of oil-in-water emulsions and its easy scale-up fabrication process indicate its great potential for practical applications.

## 2 Experimental

### 2.1 Materials

PAN ( $M_w = 85000$ ,  $\rho = 1.184 \text{ g} \cdot \text{cm}^{-3}$ ) was purchased from Jima Composites Co., Ltd. PVP (K29-32,  $M_w = 58000$ ,  $\rho = 1.144 \text{ g} \cdot \text{cm}^{-3}$ ) and Sudan red II were purchased from J&K. *N,N*-Dimethylformamide (DMF) and hexane were purchased from Xilong Scientific. Soybean oil was obtained from Jiusan Oils & Grains, Co., Ltd. 1,2-Dichloroethane and sodium dodecyl sulfate (SDS) were purchased from Aladdin. Diesel oil was purchased from China National Petroleum Corporation.

### 2.2 Methods

#### 2.2.1 Preparation of bicontinuous porous structure membranes via AA-NIPS method

The membranes were prepared via an AA-NIPS method. PAN (6 g) and PVP (10 g) powders were added to DMF (84 g) and the mixture was stirred at 50 °C for 3 h to form a transparent casting solution. After removing air bubbles, the casting solution was hand-cast onto a non-woven fabric (80–90  $\mu\text{m}$  thick, Hirose, Japan) using a casting knife with a blade height of 150  $\mu\text{m}$ . The nascent cast film was immediately treated with water mist generated by an ultrasonic atomizing humidifier (HQ-JS130H, China) for a certain time with the cast film side facing the water mist. Then the atomization pretreated cast film supported on non-woven fabric was immersed into a water coagulation bath to finish the NIPS method and the resulting membranes were stored in deionized water. The membranes prepared by different atomization pretreatment time (0, 10, 20, 30, 40, and 50 s) are respectively marked as PAN/PVP-0s, PAN/PVP-10s, PAN/PVP-20s, PAN/PVP-30s, PAN/PVP-40s, PAN/PVP-50s.

The membrane preparation procedure of PAN-30s is the same as for the PAN/PVP-30s sample except using pure PAN casting solution (6 wt% PAN, 94 wt% DMF).

### 2.2.2 Preparation of PAN/PVP membrane by other methods

**VIPS plus NIPS method:** The same casting solution as for PAN/PVP-30s sample (6 wt% PAN, 10 wt% PVP, 84 wt% DMF) was hand-cast onto a glass plate with a blade height of 200  $\mu\text{m}$ . The cast film on the glass plate was placed in an environment of 99.9% humidity at 20 °C for 10 min, and then immersed in deionized water. The cross-sectional morphology was observed after being fractured in liquid nitrogen.

**Spin coating method:** The PAN/PVP casting solution (PAN/PVP = 6/10, weight ratio) was further diluted with DMF to form a homogeneous solution of 1 wt% solid content. A drop of the solution was spin coated onto a clean silicon wafer at 10000  $\text{r} \cdot \text{min}^{-1}$  for 20 s by a spin coater (SETCAS KW-4S, China) to form a thin layer of polymer blend film. The PAN/PVP film was further vacuum dried at 25 °C for 1 h, of which the surface morphology was observed by using atomic force microscopy (AFM).

**NIPS method:** The flat membrane was fabricated by casting the casting solution (PAN/PVP = 6/10, weight ratio) onto a nonwoven fabric using a casting knife with a blade height of 150  $\mu\text{m}$ . The nascent cast film was immediately immersed into deionized water to obtain a flat film. The resulting membranes were stored in deionized water.

### 2.2.3 Emulsion separation experiment

The surfactant-free oil-in-water emulsions were prepared by ultrasonic treatment of oil/water mixture with a volume ratio of 1:9 for 1 h. Surfactant-stabilized oil-in-water emulsions were prepared by mixing oil with the 0.1 g · L<sup>-1</sup> SDS aqueous solution, with a volume ratio of 1:99, and then ultrasonic treating the mixture for 1 h. The emulsion separation experiment was carried out in the cross-flow mode using a membrane cell (CF042SS, Sterlitech Corp., USA) with an active filtration area of 42 cm<sup>2</sup> at a transmembrane pressure of 10 kPa. The permeation flux  $J$  was calculated as follows:

$$J = \frac{\Delta V}{\Delta t \times A}, \quad (1)$$

where  $\Delta V$  is the permeation water volume collected over a predetermined time  $\Delta t$ , and  $A$  is the active filtration area.

### 2.2.4 Anti-oil-adhesion coating experiment

The inner wall of a clean glass beaker was coated with PAN/PVP casting solution and then treated with water mist

generated by an ultrasonic atomizing humidifier for 30 s before being immersed in the water bath to obtain a beaker with anti-oil-adhesion coating.

### 2.3 Characterizations

The membrane morphology was characterized using a scanning electron microscope (Hitachi S-4800, Japan). The sample for cross-sectional morphology of the membrane was prepared by breaking a membrane coupon in liquid nitrogen. The pore size of the membrane was analyzed using a micro-filtration membrane porometer (GaoQ PSDA-20, China). The water contact angle (CA) and underwater oil CA were measured using a CA meter (KRUSS DSA100, Germany). The dynamic underwater oil adhesion test was conducted by using a polytetrafluoroethylene needle on DSA100. The whole testing process was recorded by a digital camera system. The oil droplet size of oil-in-water emulsions was characterized by optical microscopy (LEICA DM 2700M, Germany) and dynamic light scattering particle size analyzer (Malvern Zetasizer Nano ZS, UK). Oil content in filtrate was measured using a total organic carbon (TOC) analyzer (Multi N/C3100, Germany). The micro-phase separation of PAN/PVP was observed by using AFM (Dimension Fastscan, Bruker Co., Ltd., USA). The surface composition of membranes was analyzed by attenuated total reflectance Fourier transform infrared spectroscopy (Nicolet 6700, Thermo Fisher Co., Ltd., USA). The nuclear magnetic resonance spectra reported in this study were recorded using an Agilent 400-MR DD2 Spectrometer in DMSO-*d*<sub>6</sub> at 60 °C. Membrane porosity  $\varepsilon$ , i.e., the ratio of empty to total volume of the sample, was measured by gravimetric method [44].

$$\varepsilon = \frac{(m_1 - m_2)/\rho_w}{(m_1/m_2)/\rho_w + m_2/\rho_p}, \quad (2)$$

where  $m_1$  is the weight of the membranes infiltrated by deionized water,  $m_2$  is the weight of the dry membranes,  $\rho_w$  is the density of water, and  $\rho_p$  is the density of substrate polymer.

---

## 3 Results and discussion

### 3.1 AA-NIPS method

The construction of bicontinuous porous PAN/PVP membrane with micro/nanoscale hierarchical structure by AA-NIPS method consists of three key steps: 1) preparing polymer casting solution of PAN and PVP; 2) pretreating the nascent cast film in an atomized nonsolvent (water) droplet bath for a short period of time (A-VIPS step); 3) immersing the atomization pre-treated cast film into a water coagulation bath for complete phase separation

(traditional NIPS step). The membrane formation process of PAN/PVP bicontinuous porous structure membrane is schematically shown in Fig. 1. As the nascent cast film composed of PAN/PVP/DMF casting solution is pretreated with atomized water droplet bath, the micron-sized water droplets (Fig. S1, cf. Electronic Supplementary Material, ESM) gradually infiltrate into the casting solution, during which the evaporation of DMF solvent from the casting solution is negligible. At this step, changes in the internal structure of the casting solution are like in the VIPS process. In a general way, membrane formation process by VIPS can be subdivided into three principal stages: desolvation, demixing, and phase transformation [45]. The demixing stage is a key stage to determine the pore structure, in which the precipitant is introduced from the vapor phase to the casting solution. Because the nonsolvent introduction rate is very slow, there is basically no concentration gradient on a microscopic scale over the entire membrane cross section, and a symmetric membrane can be obtained without a dense skin on the top or bottom side of the polymer membrane [46,47]. In the atomization pretreatment step, due to the relatively slow exchange of solvent and nonsolvent, the casting solution enters a thermodynamically metastable state, and the homogeneous polymer solution gradually liquid–liquid demixes into the polymer poor phase dispersed in the continuous polymer rich phase with no concentration gradient on a microscopic scale over the entire membrane cross section. When subsequently immersed in water (the NIPS step), solvent and nonsolvent further exchange quickly, and the continuous polymer rich phase precipitates to form a microfiltration membrane with uniform 3D bicontinuous network skeleton structure through the whole membrane,

which is quite like the loofah sponge structure (inset in Fig. 1).

### 3.2 Micro-morphology and formation mechanism of micro-nano structure

Scanning electron microscopy (SEM) was used to characterize the morphology and microstructure of the cross-section and top surface of the membrane sample (Unless otherwise specified, the PAN/PVP membrane sample with bicontinuous porous structure used for characterization in this article refers to a sample prepared with an atomization pretreatment time of 30 s, marked as PAN/PVP-30s), as shown in Fig. 2. The membrane displays a symmetrical cross-section. It can be seen from the magnified SEM images of the cross-section and the top surface that a large number of nano-protrusions are distributed on the whole membrane skeleton. This is a surprising experimental finding that a micro-nano composite structure was formed on the membrane skeleton. To explore the formation mechanism of the micro-nano composite structure, a series of experiments were designed and a possible formation mechanism of the micro-nano structure was proposed based on the experimental results (Fig. 3). Firstly, the pure PAN component membrane (without PVP component) prepared via AA-NIPS method has no nano-protrusions (Fig. 3(a)), which means PVP component is related with the formation of nano-protrusions. Secondly, the PAN/PVP membrane prepared by traditional VIPS plus NIPS process (Fig. 3(b)), the nascent PAN/PVP cast film was placed in the environment of 99.9% humidity for 10 min and then immersed in water) has no nano-protrusions, which reveals that AA process is

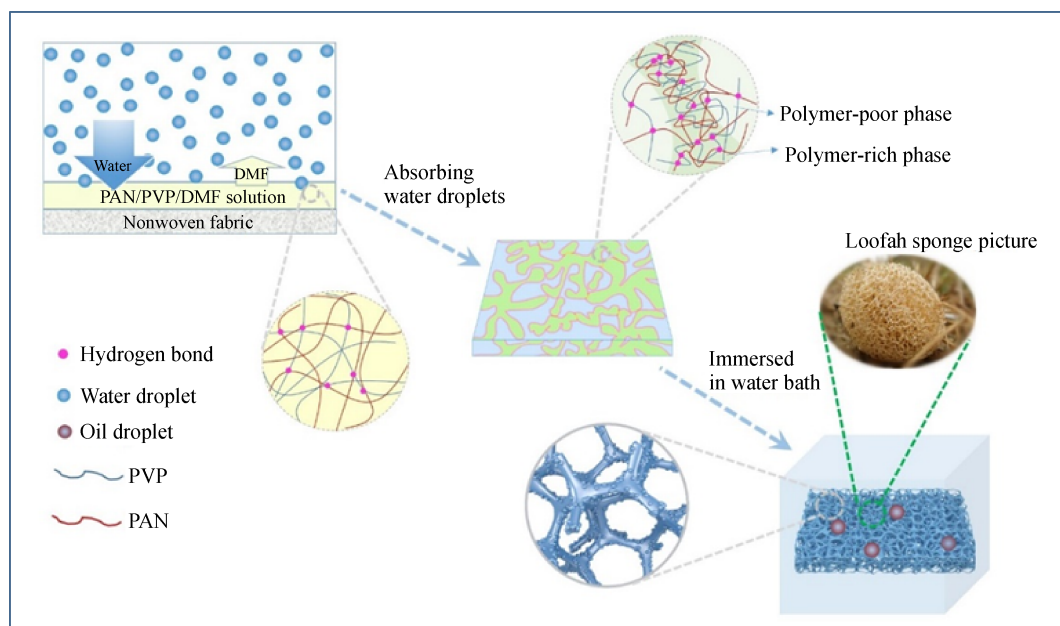


**Fig. 1** Illustration for the fabrication process of bicontinuous porous membrane by AA-NIPS method.

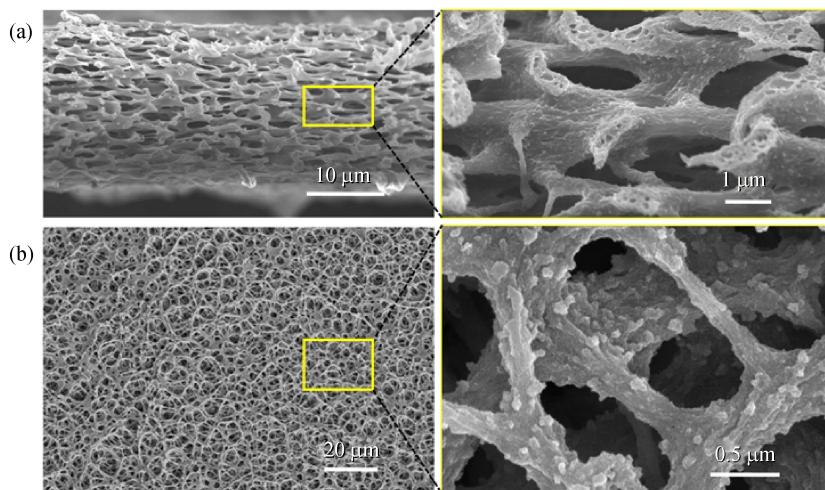


**Fig. 2** SEM images of (a) cross-section and (b) top surface of the representative membrane (PAN/PVP-30s) at different magnifications.

crucial for obtaining the nano-protrusions. Thirdly, when the atomization pretreatment time is greater than 20 s, the nano-protrusions start to appear and the number increases with increasing the atomization pretreatment time (Fig. 3(c)), which indicates that the formation of nano-protrusions is related with the infiltration of water droplets. Fourthly, the AFM image of sea island structure shows that PAN and PVP have undergone microphase separation when DMF volatilizes from the PAN/PVP/DMF casting solution (Fig. 3(d), see 2.2.4 for the production method of PAN/PVP film). Other research work of PAN/PVP hybrid system has also reported phase separation phenomenon between the two components [48]. Fifthly, there is no significant difference in AFM modulus and adhesion force between the surface nano-protrusions and nearby flat matrix on the skeleton (Fig. 3(e)), which indicates that the compositions of nano-protrusions and its nearby matrix are basically identical. Sixthly, PAN used in this work is a copolymer containing small amount of carboxylic acid (Fig. S2, cf. ESM), hydrogen bonds tend to form between the carboxyl group in PAN component and the pyrrolidone unit in PVP component [49]. As observed, when the PAN/PVP ultrafiltration membranes were prepared under the same formula and preparation conditions, the content of remaining PVP in the membrane with carboxyl-containing PAN as raw material is significantly higher than that in the sample with non-carboxyl-containing PAN as raw material (Fig. S3, cf. ESM). This result suggests that hydrogen bonding interaction has led to a stronger interaction or entanglement of the molecular chains of the two components in the PAN (with carboxylic acid)/PVP system, so the leaching of water-soluble PVP component will be significantly reduced.

Based on the above experimental evidence, we propose a possible formation mechanism of for the micro-nano composite structure as follows. During the atomization pretreatment process, the casting solution has undergone a

liquid–liquid phase separation based on the spinodal decomposition phase separation mechanism to form a bicontinuous structure, as shown in Fig. 1. With the continuous infiltration of non-solvent water droplets in the nascent cast film, the solubility parameter of the DMF/water mixed solvents changes, which will cause the deterioration of the solubility of PAN component in casting solution, but have little effect on the dissolution of PVP component [48]. As a result, the change of the solubility parameter of the mixed solvent induces the solid–liquid separation of PAN and PVP in the polymer-rich phase, i.e., PAN will first precipitate to form nano-protrusions structure. Meanwhile, it is difficult for polymer molecules to migrate due to the hydrogen bonding and chain entanglement between PAN and PVP. Therefore, only partial microphase separation occurs between PAN and PVP, while the compositions of nano-protrusions and its nearby matrix are basically identical.

Compared with the previous reports [14,50–53], the AA-NIPS method used in this work can obtain the surface of micro-nano structure more easily. Moreover, the raw materials of this work are low-cost commercially available polymer without the need for special modification, which endows the opportunity of industrial production of the novel bicontinuous porous structure membrane.

### 3.3 Superwettability of the membrane

The micro-nano composite topological structure increases the surface roughness and endows the surface with superhydrophilicity in air and superoleophobicity underwater (Fig. 4). As shown in Fig. 4(a), the membrane shows amphiphilicity to water and oil in air. When the membrane is immersed in water, the wetting property changes from superoleophilicity in air to superoleophobicity underwater. This is mainly because the water adsorbed by the membrane completely covers the membrane surface, thus

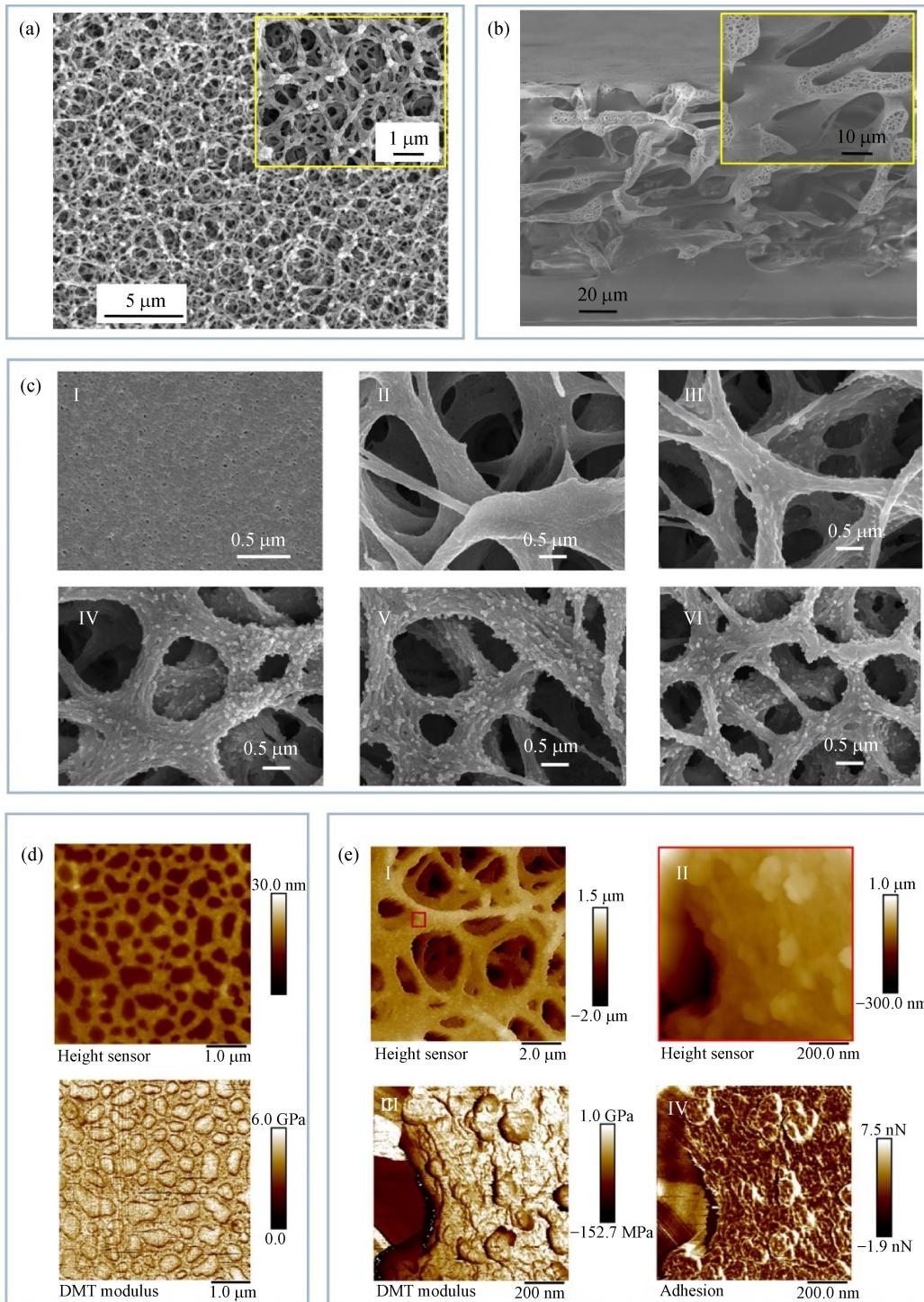


**Fig. 3** (a) SEM image of pure PAN membrane prepared by using AA-NIPS method. (b) SEM images of membrane obtained by VIPS plus NIPS method. (c) SEM images of the PAN/PVP membranes with different exposure time in water mist (I: 0 s; II: 10 s; III: 20 s; IV: 30 s; V: 40 s; VI: 50 s). (d) AFM height image and modulus image of PAN/PVP film prepared by spin coating (DMT: Derjaguin–Müller–Toporov). (e) (I) and (II) AFM height images of PAN/PVP-30s membrane at different magnifications; (III) and (IV) AFM modulus and adhesion images of B.

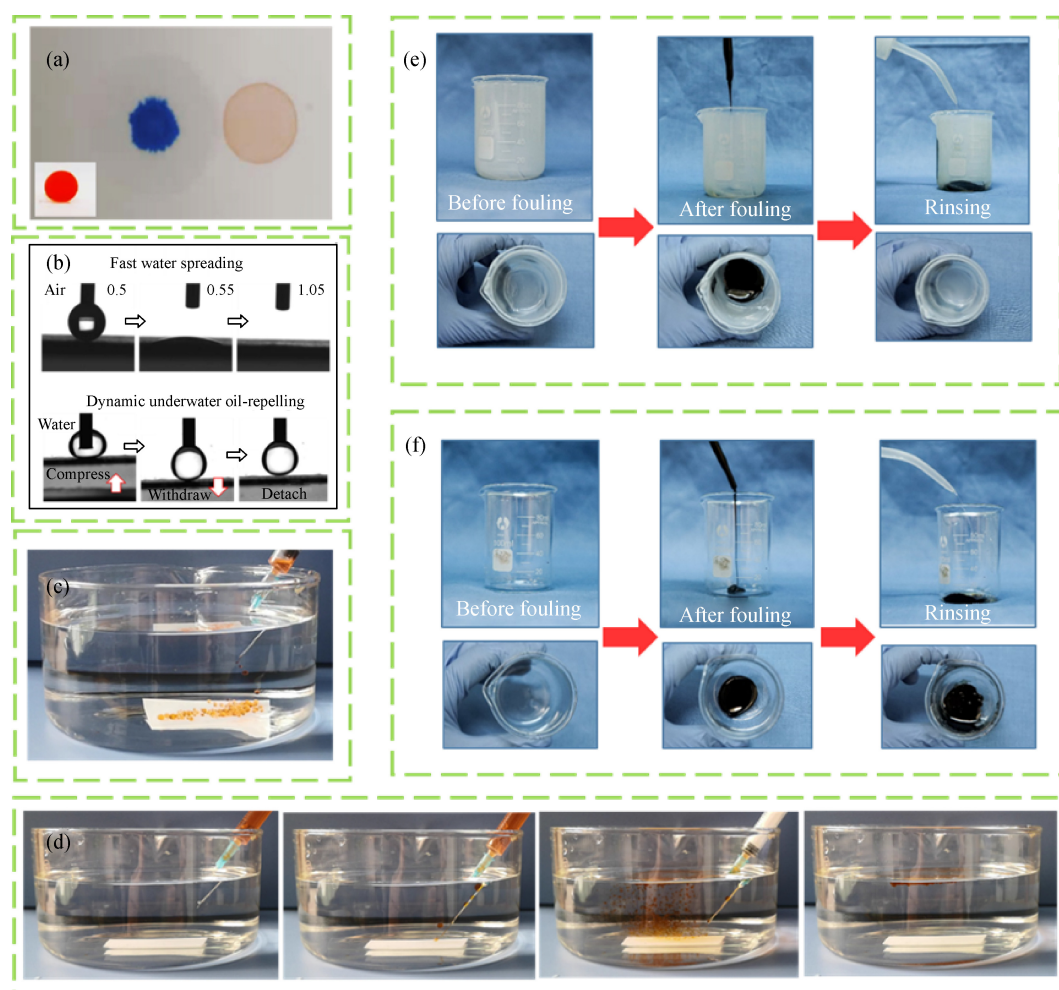


**Fig. 4** (a) Photographs of water droplet (stained with methylene blue) and oil droplet (1,2-dichloroethane stained with Sudan red II) spreading on the PAN/PVP-30s membrane in air. The inset is a digital photograph showing the 1,2-dichloroethane droplet on the membrane underwater. (b) Photographs of dynamic measurements of water spreading (top) and underwater oil-adhesion (bottom) on the membrane. Fouling experiments of PAN/PVP-30s membrane with (c) dichloroethane and (d) hexane. Crude oil fouling experiments of glass beakers coated with (e) and without (f) PAN/PVP anti-oil-adhesion layer.

forming a stable hydration layer and avoiding the direct contact between oil and membrane surface [12,23,41]. Moreover, the adhesion work of the membrane to water is significantly higher than that to oil (see section 3 in ESM), which makes it difficult for the water adsorbed by the membrane skeleton to be replaced by oil. This ensures the stability of the composite interface between the membrane skeleton and water.

A camera system with 50 frames per second was used to record the wetting behavior of the membrane. When a water droplet (3  $\mu$ L) contacts the membrane surface (Fig. 4(b), top), it spreads out quickly and a nearly zero CA is reached within one second, indicating that the membrane has excellent superhydrophilic property. Figure 4(b) (bottom) shows the photographs of the membrane touching and then leaving an oil droplet (10  $\mu$ L, 1,2-dichloroethane). In the test, the oil droplet was compressed on the membrane surface until it was significantly deformed to

simulate the contact pressure between the oil droplets and the membrane during the actual oil-water separation. Then, the membrane was slowly moved away from the oil droplet and the shape change of oil droplet was recorded when it was detached from the membrane surface. It can be found that no obvious deformation occurs during the leaving process, indicating an extremely low oil adhesion force.

Further, the underwater antifouling properties of the coating on light, heavy and crude oils were investigated respectively. A stream of dichloroethane (Fig. 4(c), dyed red) and hexane (Fig. 4(d), dyed red, Movie S1, cf. ESM) spheres can rebound from the surface of PAN/PVP-30s membrane. Movie S2 (cf. ESM) shows a drop of oil on the membrane underwater was easily removed by the injector and there was no residue left, which owes to the anti-oil-adhesion property of the membrane underwater. In addition, PAN/PVP coating layer fabricated by the AA-NIPS method can also be easily coated on many materials,

such as glass, to improve their anti-oil-adhesion property underwater. As shown in Figs. 4(e) and 4(f), the glass beaker coated with PAN/PVP layer can be simply rinsed with water to eliminate the adhesion of crude oil, while the untreated beaker is stuck with crude oil. The result demonstrated that the viscous crude oil can be removed by water rinsing easily (Movies S3 and S4, cf. ESM).

### 3.4 Influence of atomization pretreatment time on microstructure and wettability

To analyze the influence of atomization pretreatment time on the microstructure and wettability of the membrane, a series of PAN/PVP membranes were prepared by adjusting the atomization pretreatment time. As shown in Fig. 3(c), when the atomization pretreatment time is 0 s, i.e., using the traditional NIPS method, an ultrafiltration membrane with a surface pore size of 5–30 nm was obtained. With the beginning of atomization pretreatment, the pore size becomes larger and the bicontinuous porous structure appears. With the increase of atomization pretreatment time (20 s), nanoscale protrusions appear gradually on the membrane skeleton, and the number and size of nano-protrusions also increases with the increase of pretreatment time. The increase of nano-protrusions should be related to

the increasing amount of water absorbed by the cast film. The original casting solution is homogeneous. The continuous imbibition of nonsolvent by the cast film gradually deteriorates the solubility of the DMF/water mixed solvent to the polymers, resulting in the micro-phase separation of more PAN and PVP, so that more nano-protrusions are generated.

The microstructure of membrane surface has a great influence on the wetting property (Fig. 5). As shown in Fig. 5(a) (The corresponding CA images are shown in Fig. S4, cf. ESM), the water CA of the membrane without atomization pretreatment is  $42^\circ$ , and the oil CA underwater is  $106^\circ$ . When the pretreatment time increases to 10 s, the water CA decreases to  $38^\circ$  and the oil CA underwater slightly increases to  $110^\circ$ . The water CA in air and underwater oil CA change inversely with the increase of atomization pretreatment time, with the former decreasing and the latter increasing. When the atomization pretreatment time is 30 s, the membrane with many nano-protrusions on the skeleton has  $0^\circ$  water CA and  $155^\circ$  oil CA underwater, showing superhydrophilicity in air and superoleophobicity underwater. The results show that the wettability is significantly influenced by the size and distribution of nano-protrusions on the membrane. Figure 5(b) shows the membrane volume porosity

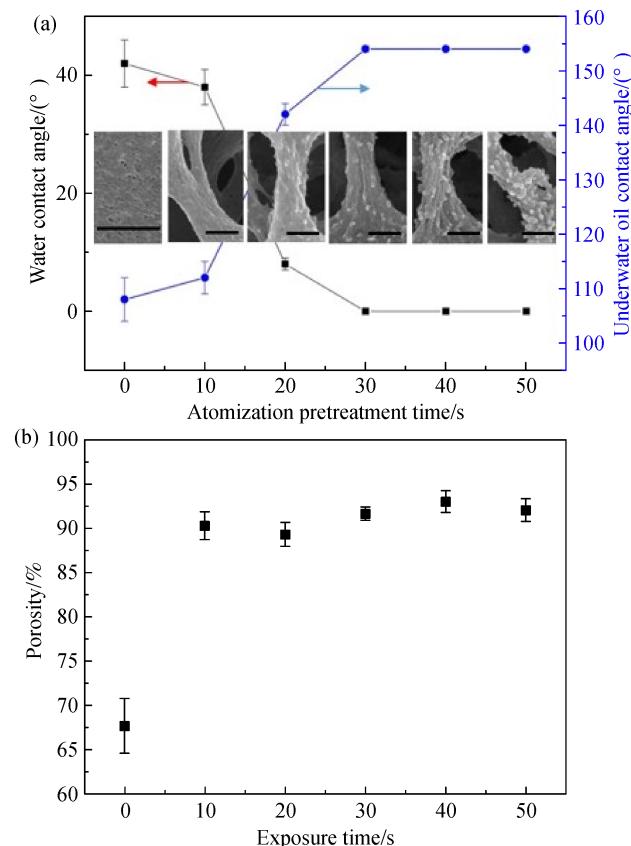


**Fig. 5** (a) Variation of water CA and underwater oil CA of the membrane with different atomization pretreatment time (The inset images are the corresponding SEM image. Scale bar: 0.5  $\mu\text{m}$ ); (b) variation of volume porosity values of the membrane functional layer.

increases from 65% to around 90% with increasing atomization pretreatment time. The high porosity of PAN/PVP samples with bicontinuous fibrous structure is very similar to the characteristic of electrospun nanofiber membrane.

### 3.5 Oil-in-water emulsions separation performance

Considering the wettability and pore structure of the membrane material comprehensively, the PAN/PVP-30s membrane was selected for oil-water separation test (Fig. 6). The average pore diameter of the membrane is 1.06  $\mu\text{m}$ . (Fig. S5, cf. ESM). As shown in Fig. 6(c), the emulsion separation experiment was carried out in cross-flow mode with a transmembrane pressure of 10 kPa. Dynamic light scattering results show that the oil droplet size ranges from 1 to 10  $\mu\text{m}$  in surfactant-free emulsions, and ranges from several hundred nanometers to 3  $\mu\text{m}$  in surfactant-stabilized emulsions (Fig. S6, cf. ESM). As shown in Fig. 6, the bicontinuous porous structure membrane with micro-nano composite structure can effectively separate different types of emulsions. The

TOC values of the relevant emulsions are shown in Table S1 (cf. ESM). For the surfactant-free emulsions, the corresponding fluxes are 3700, 2805, 2149  $\text{L}\cdot\text{m}^{-2}\cdot\text{h}^{-1}$  for hexane/H<sub>2</sub>O, diesel/H<sub>2</sub>O, soybean oil/H<sub>2</sub>O, and the TOC values of the three filtrates after one-time filtration are all lower than 5 mg·L<sup>-1</sup>, indicating their separation efficiencies are greater than 99.8%. The oil droplets of surfactant-stabilized emulsions are relatively smaller and more stable, and the surfactant will cause a certain degree of contamination to the surface and pores of the membrane, making the oil/water separation and membrane recycling more difficult [54]. The separation performance of the membrane to the three surfactant-stabilized emulsions is also shown in Fig. 6. The corresponding fluxes are 2650, 1980, and 1311  $\text{L}\cdot\text{m}^{-2}\cdot\text{h}^{-1}$ , and the TOC values in the filtrates are 32.48, 42.19, and 48.54 mg·L<sup>-1</sup>, respectively. The surfactant is soluble in water and the TOC value of the filtrate includes the influence of the surfactant passing through the membrane. In order to evaluate its influence on the TOC of the filtrate, 0.1 g·L<sup>-1</sup> SDS solution was passed through the PAN/PVP-30s membrane at 10 kPa, and the TOC of the filtrate was 18.93 mg·L<sup>-1</sup>. Therefore, if the

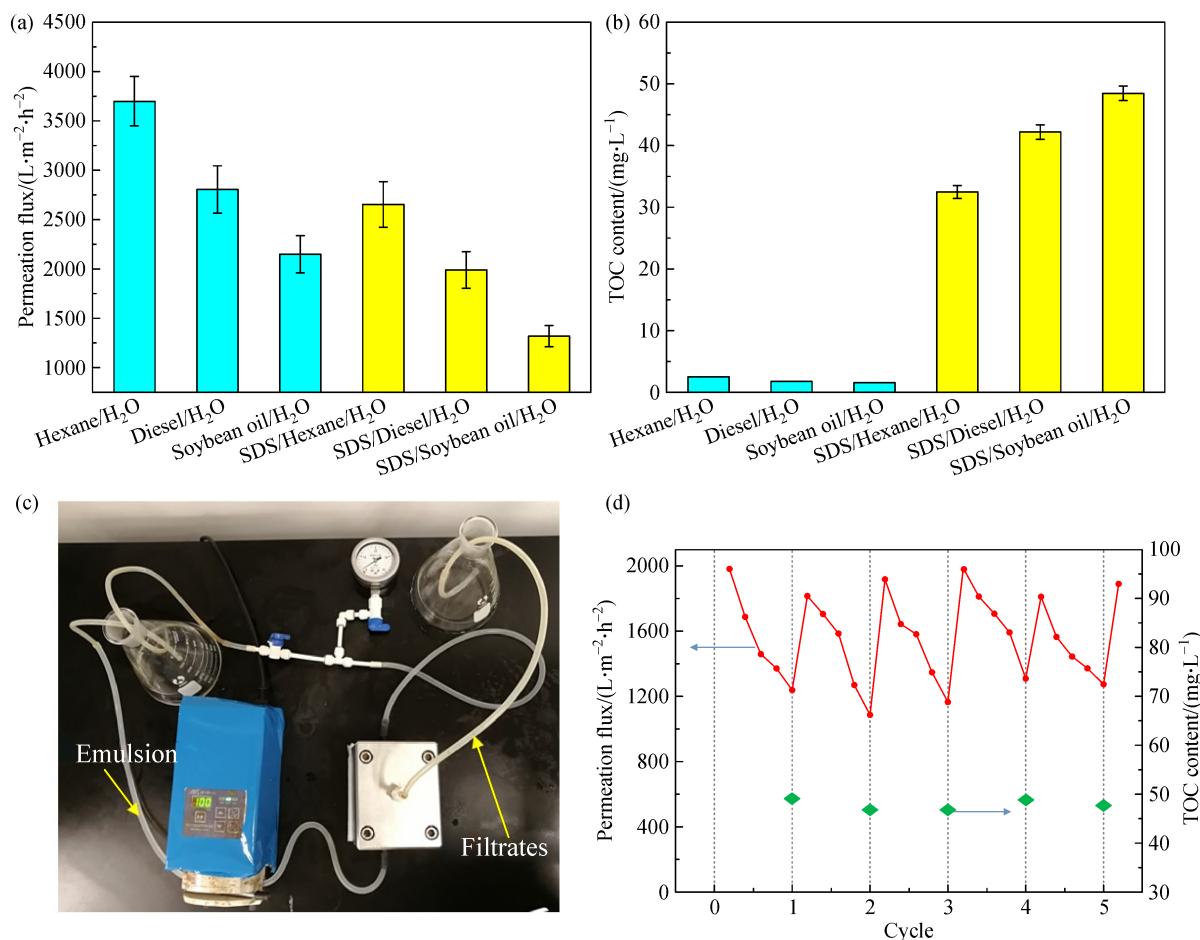


**Fig. 6** (a) Permeation flux and (b) the corresponding TOC values of the filtrates for various oil-in-water emulsions at a transmembrane pressure of 10 kPa; (c) digital photograph showing the filtration set-up of oil-in-water emulsion separation in cross-flow mode; (d) cycling separation performance of the membrane for SDS/diesel/H<sub>2</sub>O emulsion and the corresponding TOC values of the filtrates.

influence of SDS is subtracted, the actual TOC of the filtrate will be smaller and the separation efficiency will be better. As shown in Fig. S7 (cf. ESM), the milky white emulsion becomes clear and transparent after being filtered through the membrane. Optical microscope images indicate that tiny droplets of oil have been filtered out. The above results show that the membrane can effectively separate both surfactant-free and surfactant-stabilized emulsions, which proves that the membrane has significant practical value.

It is well known that a stable micro-nano composite structure is very important for the long-term use of membranes with superwettability. The surface microstructure of PAN/PVP-30s membrane was observed respectively after the membrane was soaked in deionized water for one month or ultrasonic treated in a DMF aqueous solution (DMF/water = 1/1, volume ratio) for 30 min. It is found that the surface micro-nano composite structure is basically unchanged, i.e., nano-protrusions still exist firmly on the membrane skeleton (Fig. 7). As aforementioned, only partial microphase separation between PAN and PVP occurred during membrane formation, so the macromolecular chains of the two polymers are still tightly entangled after the microphase separation. Therefore, the water-soluble PVP component is difficult to dissolve in water after long-time soaking in water environment and the nano-protrusion structure can be maintained for long time. The soaked membrane still retains its excellent underwater superoleophobicity when tested with 1,2-dichloroethane droplet (Fig. 7), indicating its long-term stability of wettability. Additionally, the existence of nonwoven fabric not only plays a role of supporting the bicontinuous porous structure functional layer, but also provides the separation membrane with excellent mechanical properties. After bending for several hundred times (500), no crack (Fig. S8, cf. ESM) was observed, which enables the separation membrane in industrial applications.

Subsequently, the cycling performance of the membrane was tested with SDS/diesel/H<sub>2</sub>O emulsion in the cross-flow mode with the transmembrane pressure of 10 kPa. As shown in Fig. 6(d), the flux was monitored hourly, and the membrane was only rinsed with deionized water after each

cycle. The water flux decreases gradually during each cycle, because the surfactant stabilized oil droplets hardly aggregate and the filter cake is formed on the membrane surface. The existence of filter cake reduces the effective filtration area of the membrane, resulting in a rapid decrease in the permeation flux. When the membrane was simply rinsed with water, its flux could be recovered to the initial state. The separation efficiency was not significantly changed during the whole cycle test process, indicating that the membrane has an excellent recyclability. This should be attributed to the excellent oil-fouling-resistant and outstanding mechanical properties.

### 3.6 Scale-up preparation process

The above experimental results have proved that the PAN/PVP microfiltration membrane made by the AA-NIPS method has excellent oil-water separation performance and long-term stability. If continuous production can be realized, it will pave the way for practical applications. For this reason, we modified the existing continuous casting equipment (DKN-40, China) in the laboratory, and successfully achieved the scale-up preparation of the PAN/PVP membrane using AA-NIPS method from the laboratory batch process to the continuous fabrication process. The process route is schematically shown in Fig. 8. By controlling the casting speed, the membrane with performance equivalent to that of the laboratory batch process was obtained, and plate-and-frame membrane modules were produced (Fig. S9, cf. ESM).

## 4 Conclusions

In summary, a superhydrophilic and underwater superoleophobic PAN/PVP bicontinuous porous structure membrane with micro-nano composite structure has been prepared by a novel AA-NIPS method. The formation mechanism of the micro-nano composite structure is proposed. The membrane can effectively separate oil-in-water emulsions at a small transmembrane pressure with high separation flux and retention rate. The underwater

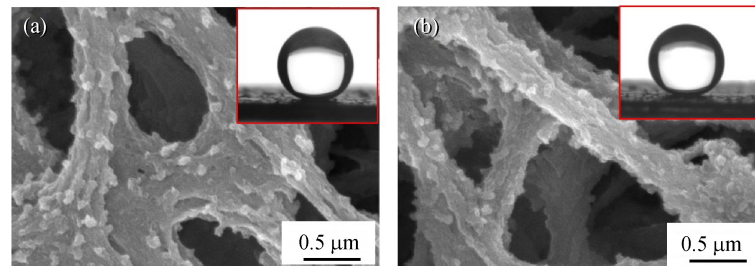


**Fig. 7** SEM images of the PAN/PVP-30s membrane after (a) soaking in deionized water for one month and (b) ultrasonic treatment in DMF aqueous solution (DMF/water = 1/1, volume ratio) for 30 min. The inset is the image of the underwater oil droplet on the corresponding membrane.

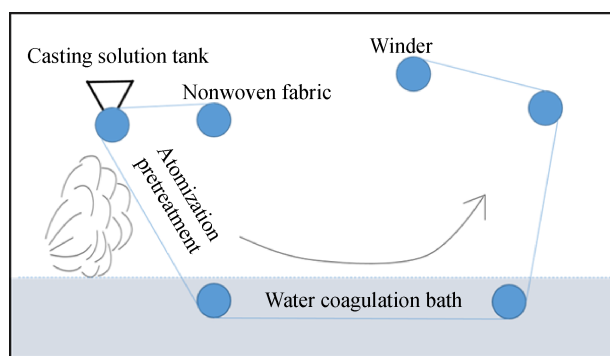


**Fig. 8** Illustration for the continuous fabrication of bicontinuous porous structure membrane by AA-NIPS method.

superoleophobicity, anti-oil-adhesion property and structural stability endow the membrane with excellent antifouling property for long-term use. The continuous production of PAN/PVP bicontinuous porous structure membrane has been achieved. In the next step, we will study the further amplification of the AA-NIPS continuous process and the application of the membrane in the fields of environmental protection, medicine, energy.

**Acknowledgements** The authors gratefully acknowledge SINOPEC for the financial support to this work.

**Electronic Supplementary Material** Supplementary material is available in the online version of this article at <https://dx.doi.org/10.1007/s11705-022-2143-5> and is accessible for authorized users.

## References

- Peterson C H, Rice S D, Short J W, Esler D, Bodkin J L, Ballachey B E, Irons D B. Long-term ecosystem response to the exxon valdez oil spill. *Science*, 2003, 302(5653): 2082–2086
- McCay D F, Rowe J J, Whittier N, Sankaranarayanan S, Etkin D S. Estimation of potential impacts and natural resource damages of oil. *Journal of Hazardous Materials*, 2004, 107(1-2): 11–25
- Shannon M A, Bohn P W, Elimelech M, Georgiadis J G, Mariñas B J, Mayes A M. Science and technology for water purification in the coming decades. *Nature*, 2008, 452(7185): 301–310
- Khatri N L, Andrade J, Baydak E N, Yarranton H W. Emulsion layer growth in continuous oil-water separation. *Colloids and Surfaces. A, Physicochemical and Engineering Aspects*, 2011, 384(1-3): 630–642
- Cambiella A, Benito J M, Pazos C, Coca J. Centrifugal separation efficiency in the treatment of waste emulsified oils. *Chemical Engineering Research & Design*, 2006, 84(1): 69–76
- Tang C, Zhao L, Guan J, Xie S X. Adsorbent preparation from oily scum for oily wastewater treatment. *Journal of Residuals Science & Technology*, 2016, 13(2): 97–103
- Song H T, Zhou L C, Zhang L J, Gao B, Wei D Z, Shen Y L, Wang R, Madzak C, Jiang Z B. Construction of a whole-cell catalyst displaying a fungal lipase for effective treatment of oily wastewaters. *Journal of Molecular Catalysis. B, Enzymatic*, 2011, 71(3): 166–170
- Le T V, Imai T, Higuchi T, Yamamoto K, Sekine M, Doi R, Vo H T, Wei J. Performance of tiny microbubbles enhanced with “normal cyclone bubbles” in separation of fine oil-in-water emulsions. *Chemical Engineering Science*, 2013, 94: 1–6
- Zhao C L, Zhou J Y, Yan Y, Yang L W, Xing G H, Li H Y, Wu P, Wang M Y, Zheng H L. Application of coagulation/flocculation in oily wastewater treatment: a review. *Science of the Total Environment*, 2021, 765: 142795
- Kota A K, Kwon G, Choi W, Mabry J M, Tuteja A. Hydroresponsive membranes for effective oil-water separation. *Nature Communications*, 2012, 3(1025): 1–8
- Abuhasel K, Kchaou M, Alquraish M, Munusamy Y, Jeng Y T. Oily wastewater treatment: overview of conventional and modern methods, challenges, and future opportunities. *Water (Basel)*, 2021, 13(7): 980
- Cheryan M, Rajagopalan N. Membrane processing of oily streams. *Wastewater treatment and waste reduction*. *Journal of Membrane Science*, 1998, 151(1): 13–28
- Lalia B S, Kochkodan V, Hashaikeh R, Hilal N. A review on membrane fabrication: structure, properties and performance relationship. *Desalination*, 2013, 326: 77–95
- Zhang W B, Zhu Y Z, Liu X, Wang D, Li J Y, Jiang L, Jin J. Salt-induced fabrication of superhydrophilic and underwater superoleophobic PAA-g-PVDF membranes for effective separation of oil-in-water emulsions. *Angewandte Chemie International Edition*, 2014, 53(3): 856–860
- Wang R X, Zhao X T, Jia N, Cheng L J, Liu L F, Gao C J. Superwetting oil/water separation membrane constructed from in situ assembled metal-phenolic networks and metal-organic frameworks. *ACS Applied Materials & Interfaces*, 2020, 12(8): 10000–10008
- Sun T L, Feng L, Gao X F, Jiang L. Bioinspired surfaces with special wettability. *Accounts of Chemical Research*, 2005, 38(8): 644–652
- Barthlott W, Schimmel T, Wiersch S, Koch K, Brede M, Barczewski M, Walheim S, Weis A, Kaltenmaier A, Leder A, Bohn H F. The *Salvinia Paradox*: superhydrophobic surfaces with hydrophilic pins for air retention under water. *Advanced Materials*, 2010, 22(21): 2325–2328
- Liu M J, Wang S T, Wei Z X, Song Y L, Jiang L. Bioinspired design of a superoleophobic and low adhesive water/solid interface. *Advanced Materials*, 2009, 21(6): 665–669
- Wenzel R N. Resistance of solid surfaces to wetting by water. *Industrial & Engineering Chemistry*, 1936, 28(8): 988–994
- Cassie A B D, Baxter S. Wettability of porous surfaces. *Transactions of the Faraday Society*, 1944, 40: 546–551
- Feng L, Li S H, Li Y S, Li H J, Zhang L J, Zhai J, Song Y L, Liu B Q, Jiang L, Zhu D B. Super-hydrophobic surfaces: from natural to artificial. *Advanced Materials*, 2002, 14(24): 1857–1860
- Wang B, Liang W X, Guo Z G, Liu W M. Biomimetic super-lyophobic and super-lyophilic materials applied for oil/water separation: a new strategy beyond nature. *Chemical Society*

- Reviews, 2015, 44(1): 336–361
23. Ge P, Wang S L, Zhang J H, Yang B. Micro-/nanostructures meet anisotropic wetting: from preparation methods to applications. *Materials Horizons*, 2020, 7(10): 2566–2595
  24. Chen C L, Du C, Weng D, Mahmood A, Feng D, Wang J D. Robust superhydrophobic polytetrafluoroethylene nanofibrous coating fabricated by self-assembly and its application for oil/water separation. *ACS Applied Nano Materials*, 2018, 1(6): 2632–2639
  25. Xu Z, Wang L, Yu C M, Li K, Tian Y, Jiang L. *In situ* separation of chemical reaction systems based on a special wettable PTFE membrane. *Advanced Functional Materials*, 2018, 28(5): 1703970
  26. Chen J J, Zhang Y X, Chen C, Xu M Y, Wang G, Zeng Z X, Wang L P, Xue Q J. Cellulose sponge with superhydrophilicity and high oleophobicity both in air and under water for efficient oil-water emulsion separation. *Macromolecular Materials and Engineering*, 2017, 302(9): 1700086
  27. Lu T, Deng Y K, Cui J X, Cao W X, Qu Q L, Wang Y L, Xiong R H, Ma W J, Lei J D, Huang C B. Multifunctional applications of blow-spinning setaria viridis structured fibrous membranes in water purification. *ACS Applied Materials & Interfaces*, 2021, 13(19): 22874–22883
  28. Chu Z L, Feng Y J, Seeger S. Oil/water separation with selective superantiwetting/superwetting surface materials. *Angewandte Chemie International Edition*, 2015, 54(8): 2328–2338
  29. Liu M J, Zheng Y M, Zhai J, Jiang L. Bioinspired super-antiwetting interfaces with special liquid–solid adhesion. *Accounts of Chemical Research*, 2010, 43(3): 368–377
  30. Su B, Tian Y, Jiang L. Bioinspired interfaces with superwettability: from materials to chemistry. *Journal of the American Chemical Society*, 2016, 138(6): 1727–1748
  31. He K, Duan H R, Chen G Y, Liu X K, Yang W S, Wang D Y. Cleaning of oil fouling with water enabled by zwitterionic polyelectrolyte coatings: overcoming the imperative challenge of oil-water separation membranes. *ACS Nano*, 2015, 9(9): 9188–9198
  32. Chang H Y, Venault A. Adjusting the morphology of poly(vinylidene fluoride-co-hexafluoropropylene) membranes by the VIPS process for efficient oil-rich emulsion separation. *Journal of Membrane Science*, 2019, 581: 178–194
  33. Zhang J C, Liu L F, Si Y, Yu J Y, Ding B. Electrospun nanofibrous membranes: an effective arsenal for the purification of emulsified oily wastewater. *Advanced Functional Materials*, 2020, 30(25): 2002192
  34. Tian M, Liao Y, Wang R. Engineering a superwetting thin film nanofibrous composite membrane with excellent antifouling and self-cleaning properties to separate surfactant-stabilized oil-in-water emulsions. *Journal of Membrane Science*, 2020, 596: 117721
  35. Reshma C R, Sundaran S P, Juraj A, Athiyanathil S. Fabrication of superhydrophobic polycaprolactone/beeswax electrospun membranes for high-efficiency oil/water separation. *RSC Advances*, 2017, 7(7): 2092–2102
  36. Xue J J, Wu T, Dai Y Q, Xia Y N. Electrospinning and electrospun nanofibers: methods, materials, and applications. *Chemical Reviews*, 2019, 119(8): 5298–5415
  37. Luo C J, Stoyanov S D, Stride E, Pelan E, Edirisinghe M. Electrospinning versus fibre production methods: from specifics to technological convergence. *Chemical Society Reviews*, 2012, 41(13): 4708–4735
  38. Tsai H A, Kuo C Y, Lin J H, Wang D M, Deratani A, Pochat-Bohatier C, Lee K R, Lai J Y. Morphology control of polysulfone hollow fiber membranes via water vapor induced phase separation. *Journal of Membrane Science*, 2006, 278(1-2): 390–400
  39. Venault A, Chiang C H, Chang H Y, Hung W S, Chang Y. Graphene oxide/PVDF VIPS membranes for switchable, versatile and gravity-driven separation of oil and water. *Journal of Membrane Science*, 2018, 565: 131–144
  40. Ismail N, Venault A, Mikkola J P, Bouyer D, Drioli E, Kiadeh N T H. Investigating the potential of membranes formed by the vapor induced phase separation process. *Journal of Membrane Science*, 2020, 597: 117601
  41. Park H C, Kim Y P, Kim H Y, Kang Y S. Membrane formation by water vapor induced phase inversion. *Journal of Membrane Science*, 1999, 156(2): 169–178
  42. Zhao Q, Xie R, Luo F, Faraj Y, Liu Z, Ju X J, Wang W, Chu L Y. Preparation of high strength poly(vinylidene fluoride) porous membranes with cellular structure via vapor-induced phase separation. *Journal of Membrane Science*, 2018, 549: 151–164
  43. Maggay I V, Suba M C A M, Aini H N, Wu C J, Tang S H, Aquino R B, Chang Y, Venault A. Thermostable antifouling zwitterionic vapor-induced phase separation membranes. *Journal of Membrane Science*, 2021, 627: 119227
  44. Rastgar M, Bozorg A, Shakeri A. Novel dimensionally controlled nanopore forming template in forward osmosis membranes. *Environmental Science & Technology*, 2018, 52(5): 2704–2716
  45. Zeman L J, Zydny A L. *Microfiltration and Ultrafiltration: Principles and Applications*. New York: Marcel Dekker Inc., 1996, 51–59
  46. Strathmann H, Kock K. The formation mechanism of phase inversion membranes. *Desalination*, 1977, 21(3): 241–255
  47. Xu M H, Xie R, Ju X J, Wang W, Liu Z, Chu L Y. Antifouling membranes with bi-continuous porous structures and high fluxes prepared by vapor-induced phase separation. *Journal of Membrane Science*, 2020, 611: 118256
  48. Jiang Y F, Fang D W, Song G Q, Nie J, Chen B L, Ma G P. Fabrication of core-shell nanofibers by single capillary electrospinning combined with vapor induced phase separation. *New Journal of Chemistry*, 2013, 37(9): 2917–2924
  49. Yuan X F, Jiang M, Zhao H Y, Wang M, Zhao Y, Wu C. Noncovalently connected polymeric micelles in aqueous medium. *Langmuir*, 2001, 17(20): 6122–6126
  50. Ge J L, Zong D D, Jin Q, Yu J Y, Ding B. Biomimetic and superwettable nanofibrous skins for highly efficient separation of oil-in-water emulsions. *Advanced Functional Materials*, 2018, 28(10): 1705051
  51. Li X P, Shan H T, Zhang W, Li B A. 3D printed robust superhydrophilic and underwater superoleophobic composite membrane for high efficient oil/water separation. *Separation and Purification Technology*, 2020, 237(27): 116324
  52. Mähringer A, Hennemann M, Clark T, Bein T, Medina D D. Energy efficient ultrahigh flux separation of oily pollutants from water with

- superhydrophilic nanoscale metal-organic framework architectures. *Angewandte Chemie International Edition*, 2021, 60(10): 5519–5526
53. Jiang X B, Shao Y, Li J, Wu M, Niu Y, Ruan X, Yan X, Li X, He G. Bioinspired hybrid micro/nanostructure composites membrane with intensified mass transfer and antifouling for high saline water membrane distillation. *ACS Nano*, 2020, doi: 10.1021/acsnano.0c07543
54. Tummons E N, Chew J W, Fane A G, Tarabara V V. Ultrafiltration of saline oil-in-water emulsions stabilized by an anionic surfactant: effect of surfactant concentration and divalent counterions. *Journal of Membrane Science*, 2017, 537: 384–395